Imaging the Gutenberg Seismic Discontinuity beneath the Oceanic Crust of the North American Plate

Robbie Burgess

11-25-15

Dr. Nicholas Schmerr

GEOL 394

1. Abstract:

The lithosphere-asthenosphere boundary (LAB) is a rheological interface and thermally controlled boundary between the rigid lithosphere, and the more plastic Asthenosphere. Studying this boundary is essential to understanding plate tectonics and the evolution of the earth. At this boundary, a seismic can be inferred from seismic data. This discontinuity is sometimes referred to as the Gutenberg discontinuity (G), and is the name I will be using to describe this discontinuity. There are many seismic studies that have looked for the lithosphere-asthenosphere boundary beneath the North American plate. These studies have used methods with receiver functions which utilize the change from S to P waves and P to S waves when they pass through an interface. For this study, however, I examined SS precursor arrivals to determine the depth of the G. In order to obtain the SS precursor data, I collected a seismic dataset that consisted of earthquakes that sampled beneath the North American oceanic crust. To look for data that would be compatible with this project, several criteria had to be outlined. For example, I only used earthquake events that occurred shallower than 35 km depth to avoid depth phase interference with the SS precursors. Also, I only used earthquakes with a moment magnitude $\geq$ 5.8 to ensure SS had sufficient energy to fall above the background noise. Once collected, I processed the raw data in order to turn it into a usable data set I could begin studying. This processing was done by removing the instrument response and rotating the horizontal components to the back azimuth of the earthquake to get the transverse component of motion. Additionally, I filtered the raw data with a Butterworth bandpass filter with corner frequencies of 0.06 and 0.02 Hertz to remove the micro-seismic noise band above 0.06 Hertz, and long period noise above 0.02 Hertz. Afterwards, I evaluated the quality of each earthquake by examining the data for the presence of the SS seismic phase. This step involved a visual examination of the data to determine the quality of the SS arrival and to remove events that did not have a well-developed SS arrival. Next, I created vespagrams to analyze the arrivals. This step allowed me to combine information from multiple stations by stacking their energies into a single vespagram. The subsequent examination of the relative travel time and amplitude of the G-related SS precursor on each vespagram allowed me to constrain the depth and seismic impedance contrast at the boundary. I used this information to create a map showing the lateral variation in the depth of the G discontinuity beneath the North American oceanic crust. The results from this study conclude that there is a good detection of the G in this area. It has also found that there is no correlation between the depth of the G and the age of the overlying crust.

Table of Contents:

2. Introduction

Geophysics, geochemistry, and particularly seismology provide access to the Earth's deep interior. Seismic waves passing through the Earth interact with seismic discontinuities at depth. Seismic discontinuities are defined as an increase or decrease in the seismic wave velocities and density over a relatively short depth increment. Figure 1.1, from Heit et. al. (2010), is a velocity versus depth model showing some major seismic discontinuities in the upper 1000 km of the mantle. In this model, major discontinuities can be seen at around 50km, 120km, 210km, 410 km and 660km. Reasons behind the discontinuities presence have mostly been determined. The Mohorovičić Discontinuity around 50 km is a transition in the composition of the crust to the mantle while the 410 km and 660 km discontinuities are from phase changes in the mineral olivine. Other discontinuities like the one found at the mantle-outer core boundary is from the transition of rock to liquid metal. However, there are several discontinuities other than those listed above that do not necessarily have a clear explanation and remain quite enigmatic. In this study, I will be focusing on the seismic discontinuity associated with the lithosphere-asthenosphere boundary at around 50-120 km depth called the Gutenberg discontinuity (Schmerr 2012).

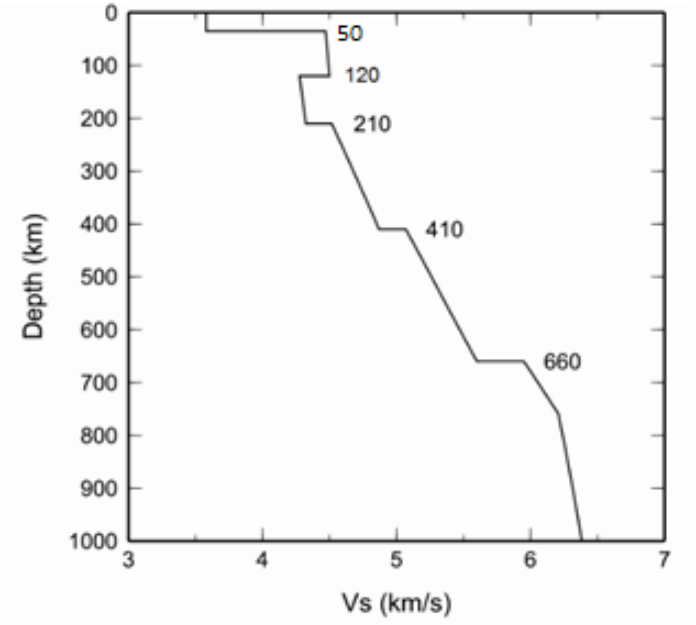

Figure 1.1: Seismic Velocity vs. Depth graph showing major seismic discontinuities within the upper 1000 km of the mantle.

The Earth's mantle is divided into layers according to seismic velocity variations detected by the propagation of body waves. Unlike the mechanisms proposed for many other discontinuities, the LAB is defined with regards to rheology, with the lithosphere behaving as an elastic solid and the asthenosphere deforming as a viscous fluid (Barrell 1914). Since then, additional definitions of the term lithosphere have been introduced such as thermal, seismic or chemical lithosphere. Observations from the high seismic velocity mantle lid are interpreted as being indicative of the seismic lithosphere (Heit et. al. 2010).

2.1 Seismology and SS Precursors

Seismology is a branch of geology that studies earthquakes and seismic waves that move throughout the earth. A great majority of earthquakes occur along faults that make plate boundaries. Since the edges of these plates are rough, they get stuck while the rest of the plate keeps moving. When the plate has moved far enough, the edges of these plates unstick on one of the faults and there is an earthquake, which forms elastic waves that propagate through the earth's interior. These wave energies can be recorded all over the earth's surface using seismometers. There are two types of waves formed by earthquakes; P waves, or compressional waves, which vibrate parallel to the direction the wave is traveling, and S waves, which vibrate perpendicular to the wave's direction of propagation. These waves are important to study because we can get an idea of how the interior of the earth looks like, since we cannot physically look into it ourselves.

Seismic discontinuities in the crust and upper mantle produce both reflections and mode conversions of seismic body waves. Examples include receiver functions, which are P to S converted phases below a seismic station. This method is applicable mostly on continents or islands where seismic stations are present. SS precursors are underside reflected SS waves from mantle discontinuities below SS bounce points, located in remote areas halfway between earthquakes and receivers and therefore can be used to globally map the mantle discontinuities. Flanagan and Shearer (1998) have shown, for example, the potential to investigate the mantle discontinuities by globally stacking SS precursor data. The primary advantage of the SS precursors over other methods is that they enable us to sample relatively large areas where no stations are deployed. This global view can help to improve the quality and resolution of upper-mantle discontinuities and understand their distribution in correlation with different tectonic regions (Deuss, 2009).

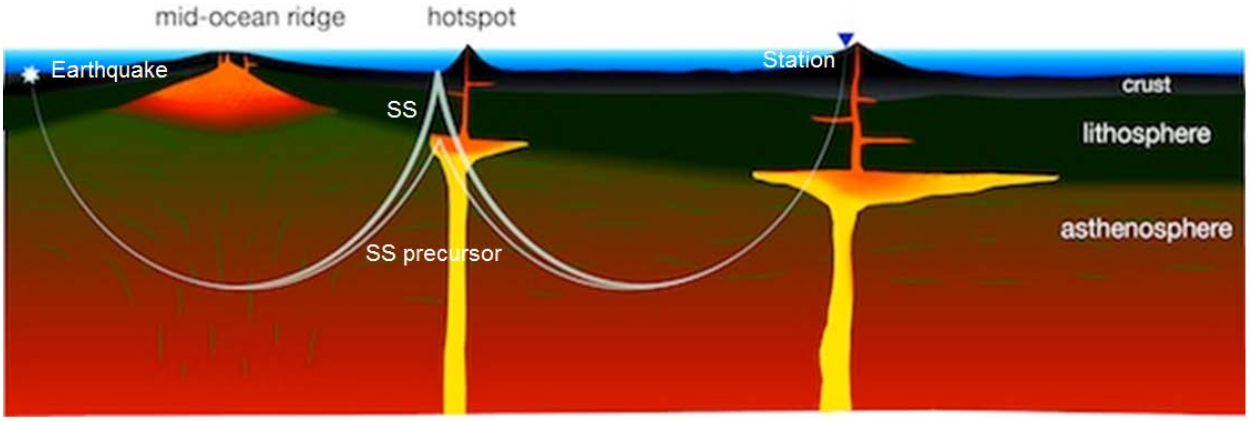

Figure 1.2: Cross section of the earth's upper interior showing the ray travel path of SS and SS precursors.

For this study, I focused on a class of seismic phases, called the SS precursors. A SS wave is an S wave that has traveled from the source, reflected once off of the earth's surface, and then was received by a seismometer station. The SS precursors are similar, however, they reflect once from a discontinuity boundary before reaching the seismometer station. Figure 1.2 shows the predicted ray paths of SS and SS precursors within the earth's interior. Due to the difference in travel distances and velocities, these two waves will reach the seismometer station at different times. This difference can be seen and studied to obtain information on the discontinuities depth.

2.2 Previous Work

Many studies have been done that analyze long period shear-wave underside reflections. Early work by Gu et. al. (1998) as well as Flanagan and Shearer (1998) used the precursors to analyze the global upper mantle discontinuities at 410 km and 660 km depth. The primary results of these papers are that the 410 km and 660 km discontinuities are global features with ± 15-20 km of relief on the boundaries. They showed the long wavelength pattern of 410 km topography was reasonably correlated with the seismic velocity perturbations in the mantle above it. They also found the global topography of 660 km was strongly correlated with shear-wave velocity variations in the transition zone. They conclude that the poor correlation between the observed topography of the 410 km and 660 km discontinuities as inconsistent with a simple model of large scale, whole mantle flow, which would imply a more complex pattern (Gu et. al. 1998). Much of the work with the SS precursors has focused on imaging of the topography of the 410 km and 660 km discontinuities.

Shearer (2000) supports the use of SS precursors with his study on upper mantle seismic discontinuities. After completing the study, he explained the importance of the SS precursor analyses was to provide direct observational constraints on the amplitude and pattern of discontinuity topography. He offers, models of topography on the transition zone discontinuities are likely to continue to improve as more seismic data are analyzed. He elucidates an important step will be to perform joint inversions of discontinuity SS precursor times with mantle tomography data sets to produce unified models of discontinuity topography and three dimensional velocity variations (Shearer 2000).

More recently, the SS precursors have been applied to shallower, more regional discontinuities. A study by Heit et. al. (2010) uses SS precursors to study the lithospheric and upper-mantle discontinuities beneath eastern Asia. They found the best traces for the LAB are located beneath the crust-mantle boundary beneath the Tibetan plateau at a depth of about 120 km and become weaker and shallower beneath eastern China. Compared to other studies, the LAB depth variation observed by Heit et al., (2010) is consistent with surface wave tomography (Huang et al. 2003; Priestley & McKenzie 2006) and receiver function studies (Kumar et al. 2006; Sodoudi et al. 2006; Chen et al. 2006, 2008). These studies generally agree that the lithosphere is thick in Tibet and west China and thins to less than 70 km beneath eastern China. They discover that the strongest and deepest LAB beneath Tibet is also consistent with the high-velocity lid shown in the background tomography (Kustowski et al. 2008) as they detected a high-velocity structure possibly related to the Indian lithosphere under-thrusting the Asian lithosphere. This variation reflects the importance of further studies to constrain and better determine the depth of the LAB (Heit et. al. 2010).

Detections of a shallow seismic discontinuity from 50-80 km depth are shown to exist beneath the Pacific Ocean in Schmerr (2012). In this study, high-frequency SS precursor sampling beneath the Pacific plate showed that the G is intermittently detected as a sharp, negative velocity contrast at 40 km to 75 km depth. These observations are detected near the depth of the LAB in regions associated with recent surface volcanism and mantle melt production. The G is interpreted to be occurring in the vicinity of an intermittent layer of asthenospheric partial melt residing at the lithospheric base. Schmerr (2012) proposes that the G reflectivity is regionally enhanced by dynamical processes that produce melt, including hot mantle upwelling, small-scale convection, and/or fluid release during subduction.

3. Project Statement and Hypothesis

By mapping the Gutenberg discontinuity with the SS precursors, I would like to determine where the G discontinuity lies beneath the North American oceanic plate, and whether or not it is consistent with the LAB. To do this, I will be using SS precursor data to map the lateral variations in the depth and impedance contrast at the discontinuity. It is from this map that I was able to test my hypothesis. My hypothesis is that if the oceanic Gutenberg discontinuity is consistent with the lithosphere-asthenosphere boundary, then the depth of the discontinuity will show a strong crustal age correlation in its depth. More simply put, if I assume the G follows the LAB, I would expect the depth of the G to increase as the age of the overlaying plate increases. This is because as a plate moves away from a ridge, it cools and the lithosphere thickens, effectively increasing the depth at

which the LAB is found. An image showing how the thickness of an oceanic plate increases as it moves away from its respective ridge can be seen in Figure 2.

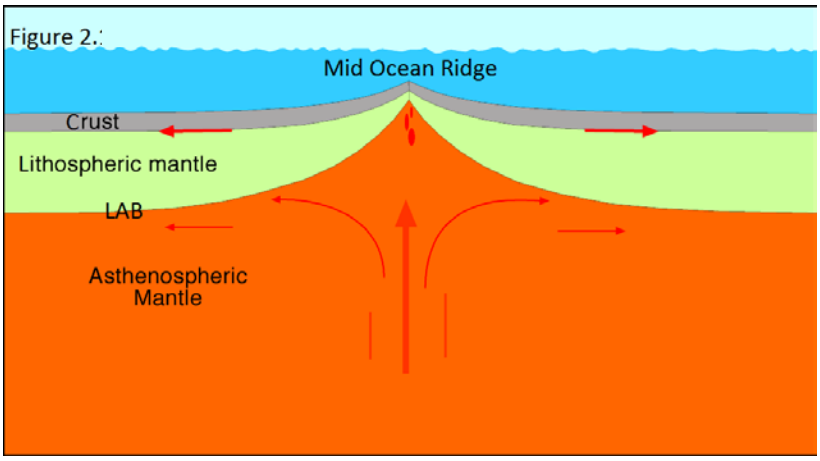

Figure 2: Cross section of the Mid Ocean Ridge (MOR) showing how the depth of the LAB increases as it moves farther away from the center of the Mid Ocean Ridge (DiVenere, 2013)

The broadest implication of this work is to add to the overall arching body of geologic knowledge. As previously stated, a lot of information on the origin and driving forces behind the Gutenberg discontinuity remains under debate. I am using SS precursor data to probe beneath the North American side of the Atlantic Ocean, a region that has not yet been studied with SS precursors. Additionally, new theories can be produced using the digital map I have created. I can compare the results I have gathered with other studies of related topics. SS precursors have been used to map the G beneath the Pacific plate, as well as discontinuities that lie deeper within the earth. By comparing my results with the ones found in other studies like Gu et. al. (1998) and Flanagan and Shearer (1998), I can compare and contrast the G in relation to continental and oceanic plates. I will also be able to compare results with the studies using receiver functions. Not only is my study useful for finding the G beneath North America, but the research will help confirm or add to the hypotheses that other discontinuity studies already made.

4. Experiment Design and Methods

This rigorous study had many intricate components. I have separated these components into five major steps in order to more clearly explain and visualize the work done in this study. The first step, collecting the data, involves gathering heavily constrained data from the Incorporated Research Institutions for Seismology. The next step, processing the data, turns the collected raw data into a useable data that can be studied. The third step, hand picking events, involves physically going through the processed data to select precursor information. The subsequent step utilizes the array method of velocity spectral analysis, or vespagram. These vespagrams amplify the SS precursor arrivals out of the noise levels and show the depths and amplitudes of discontinuities (Schmerr, 2011). Finally, from the resolved vespagrams, I am able to assess the depths where the G discontinuity lies. This process is outlined in figure 3.1.

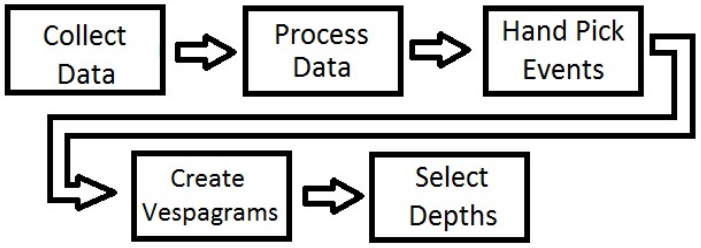

Figure 3.1: A flow chart breaking down the methods of this study into five major steps.

4.1 Data selection

In order to begin, I had to gather seismograms which I would later be able to process. To construct the dataset of usable seismograms, I first had to get the seismic data from the Incorporated Research Institutions for Seismology (IRIS), a publically accessible database for seismic data. In order to receive the most useful information, I had to set strict parameters on which types of earthquake events I needed. First, the event had to occur within the past 25 years (1990-present). This time constrain was placed to make sure that there was enough stations deployed at the time of the earthquakes. Also, I restricted the event depths below 35 km to limit the interface of depth phases of earlier arriving phases with the precursor wave-field. I also restricted the source magnitudes greater than 5.8 to ensure a good signal to noise ratio for the SS phase (Schmerr et. al. 2006). Approximately 1800 earthquake events meet the criteria for source magnitude and depth. However, the most important parameter was selecting earthquake and seismometer pairs that had SS arrivals sampling beneath the North American oceanic crust. This brought the number of earthquake events down to about 40 events. Once I knew which events I would be using for this study, I requested the raw data from IRIS which I could then process.

4.2 Data Processing

The next step was to take the raw earthquake data and process them. The script for this effectively cleaned the raw data so it was more easily dissected. This process has four tasks. First, it uses the SACPZ files, included with the raw data from IRIS, to match each record with a pole zero file to remove instrument response. It decides whether or not a record has a good pole zero file, if it does the instrument response is removed and if not, the record is dumped into a backup directory. Once the response is removed, it looks at the files to make sure they are not under sampled. For

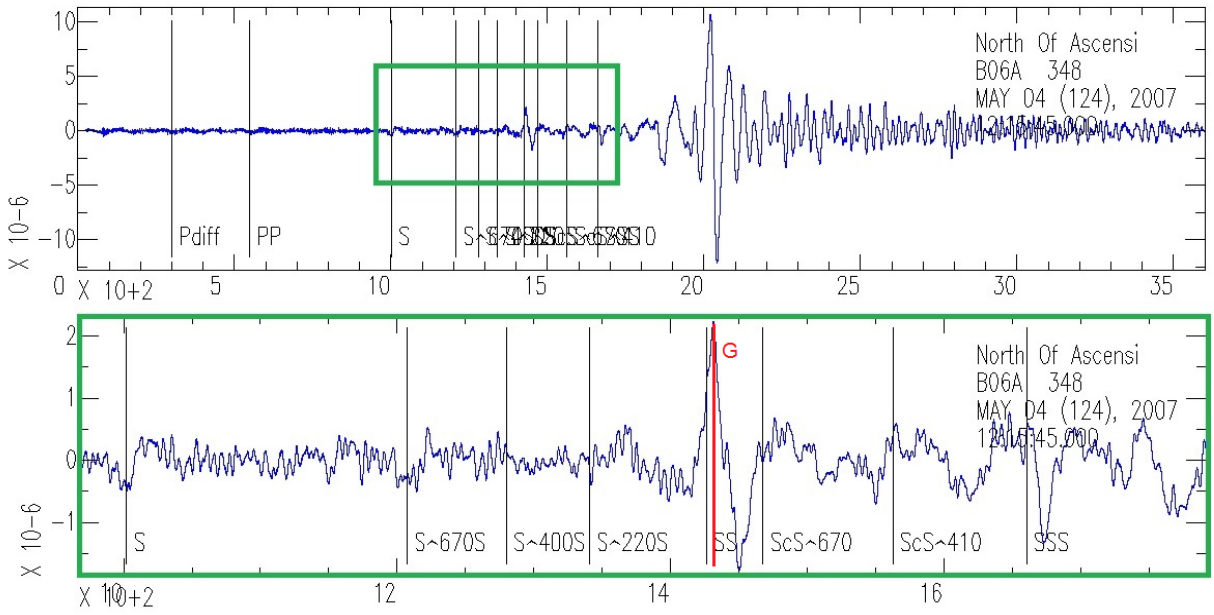

Figure 3.2: Example seismogram after it has been processed. The top seismogram shows the entire seismogram. The lower seismogram shows the green box zoomed in to better see the SS and discontinuity arrivals, denoted as S^670S, S^400S. The redline indicates where the G should arrive.

this, I set the minimum number of sample points to 75000 to ensure the data would be useful. Next, I had to rotate the stations to the great circle path. Doing this rotates the seismic stations into the back-azimuth of the station-earthquake pair in order to obtain the transverse component of the incoming waves. The final step in processing creates heading labels for each discontinuity on each seismogram. It does this by making a selection on the seismograms. These selections were based on their ray travel path and the time it took them to travel that path. The example seismogram in figure 3.2 shows how the data looks after it has been processed.

4.3 Hand Picking Events

Hand picking involved physically going through each seismogram for each event and selecting where I believed SS to be. This step required visually examining 1984 seismograms. If I saw the record was unusable, I could select it to be removed entirely. I looked for several things when deciding whether or not a record could be used. First, I eliminated any seismograms with any gaps. Next, I threw out any record that clearly did not follow the typical pattern of a seismogram. Lastly, I visually inspected each seismogram to reject those with no SS or poor quality SS arrivals. Once I finished hand picking, I could then determine if there was a sufficient number of stations to break the bounce point distribution out into multiple bins. This quality check left me with 7 out of my original 40 events. Table 1 shows information regarding the 7 events I used. Once I made picks on each record, I used the acceptable records to create a vespagram for each event.

Event Date	Event Longitude	Event Latitude	Event Depth (km)	Number of Stations	Average Bounce Point Longitude	Average Bounce Point Latitude
6/7/2015	-17.16	-35.36	10	164	307.65	26.27
5/24/2015	-14.17	-16.86	10	427	299.14	12.48
3/29/2014	-21.92	-0.85	12	139	309.12	44.92
11/22/2008	-14.02	-1.19	8	445	302.29	26.81
8/28/2008	-17.44	-0.024	4.5	240	314.64	48.88
4/24/2008	-23.52	-1.15	10	110	306.87	44.16
5/4/2007	-15.05	-1.35	10	459	302.85	31.48

Table 1: Information regarding the seven events used in this study which show their locations and their bounce point's locations. Longitude and latitude information is in decimal degrees.

4.4 Vespagrams

Once picks were made on each record I made interpretations on the data using vespagrams. A vespagram is an array method using velocity spectral analysis, shortened to vespagram. These vespagrams amplified the SS precursor arrivals out of the noise levels and showed the depths and amplitudes of discontinuities. They estimated the seismic energy arriving at the array for a given back azimuth and different horizontal slowness's. Slowness is the inverse of velocity, meaning I can determine a wave's travel time by multiplying the ray travel distance by its slowness. Depending on how many stations recorded the event, each event could have multiple bins which gave me bounce points at different locations. Bins were created by grouping closely distanced stations to make a global, evenly spaced grid of initial locations. There was a sufficient number of stations to break the bounce point distribution out into multiple bins, giving me sampling at 21 geographically separated points. In order to normalize amplitude, I applied several filters to data. There are two types of

filters that I ran, a high-pass filter and a low-pass filter. These filters remove amplitudes that are either larger or smaller than that designated in each pass. Filtering the data allowed me to clearly see discontinuity amplitudes while removing background noise. Two example vespagrams are presented in figure 3.3 below.

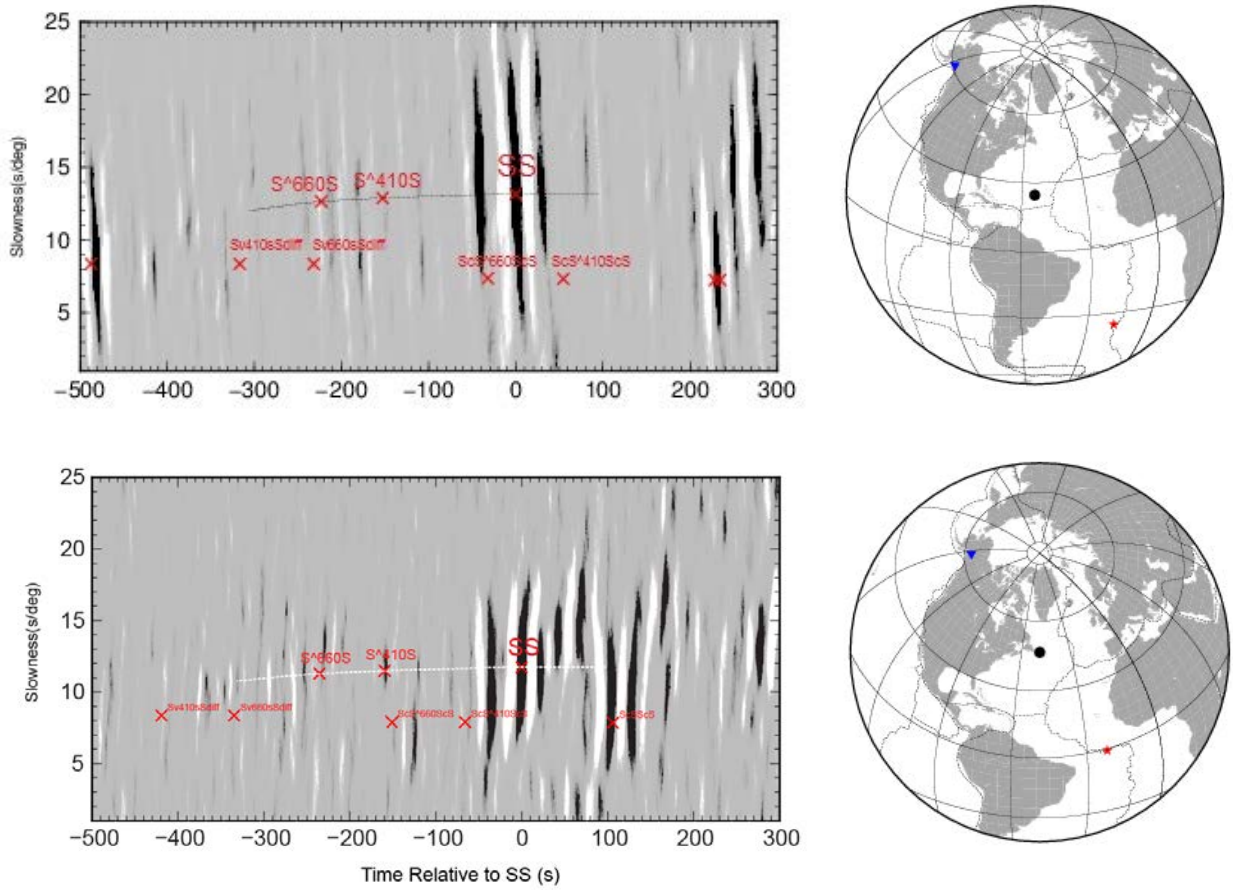

Figure 3.3: The top vespagram was formed from a bin from an earthquake in the southern mid atlantic ridge that occurred on 2015-06-17. The bottom vespagram was formed from a bin from an earthquake in the southern mid atlantic ridge that occurred on 2015-05-24. The X-axis represents time relative to SS in seconds, and the Y-axis represents the slowness in seconds per degree. On the global map, the blue triangle represents the stations, the red star represents the earthquake source, and the black dot represents the area it is sampling.

In figure 3.3, the white horizontal line is the predicted arrival slowness we would expect for these events. To predict where the precursors should arrive, I used a reference model. This model estimated where the SS and precursors should arrive in time and slowness. After looking at where they should arrive, I looked at the vespagram to see if seismic energy arrived around those predictions. The white and black vertical lines show amplitudes of differing arrivals at differing slowness's. For these events, we see a lot of energy around the SS arrival. Following the white line backwards, and getting deeper in the earth, energy can be seen around where I would expect the 410 km and 660 km discontinuities. Out front of the SS is where the Gutenberg discontinuity lies. These diagrams show solid evidence that the G does exist. The next step gives a better understanding of these diagrams by creating a new trace interpretation diagram.

4.5 Selecting Discontinuity Depths

Picking the depths at which these discontinuity lies could only be determined once I resolved the trace on the vespagrams. To do this, I made a plot of the profile and picked where the depths of the G, 410 km and 660 km discontinuities lied. This was done for every bin in each event. This pick, however, brought some uncertainty. This error was resolved by looking at the variation in the vespagrams on slowness's about 2 seconds per degree above and below the expected slowness for the G precursor. After the pick was made, I made a global map of where the station, earthquake source, and sample point were located. Two examples of the created diagrams and maps can be seen below in Figure 3.4.

Most importantly, on these diagrams we see the G around 110km deep for the 2015 event

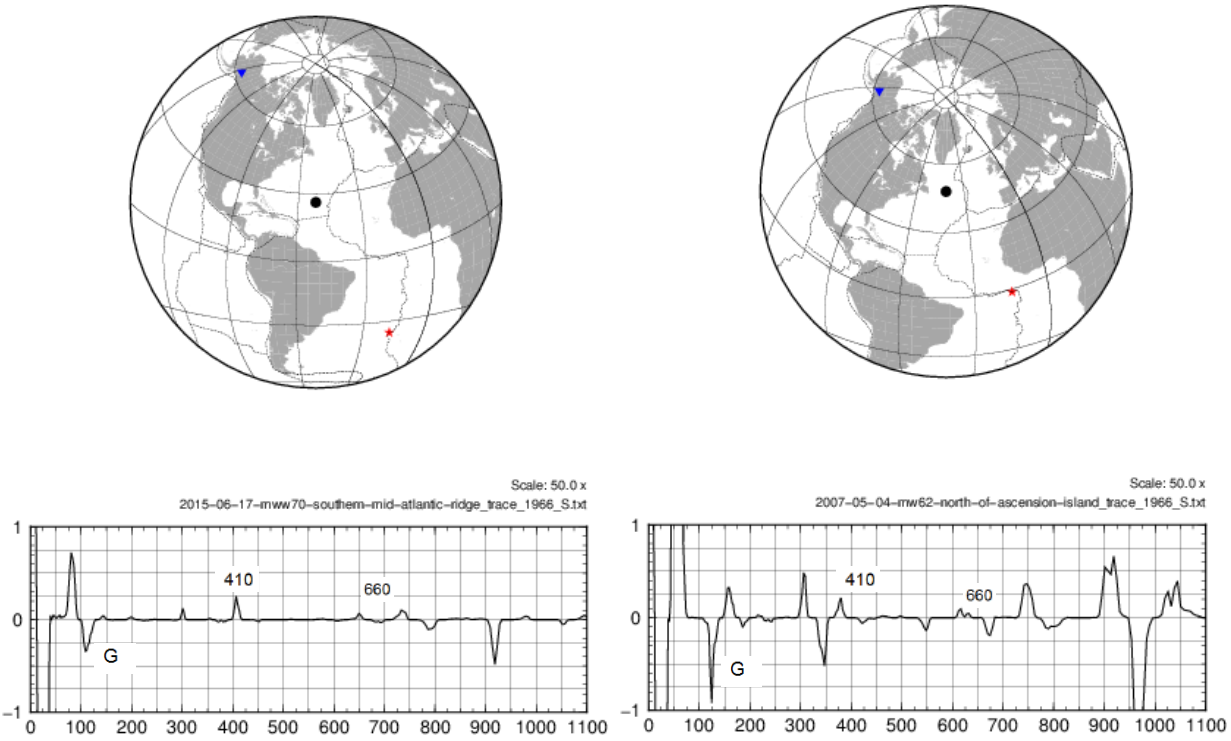

Figure 3.4: The event on the left was formed from a bin from an earthquake in the southern mid atlantic ridge that occurred on 2015-06-17. The event on the right was formed from a bin from an earthquake just north of the Ascention Islands that occurred on 2007-05-04. On these diagrams, the X-axis shows depth and the Y-axis shows amplitude. On the global map, the blue triangle represents the stations, the red star represents the earthquake source, and the black dot represents the area it is sampling.

and we see the G around 120km deep for the 2007 event. These diagrams let me see the depths at which the G and other discontinuities lie. I can also see their distance from the mid ocean ridge. With this information, I was able to make interpretations about how the Gutenberg discontinuity is laying beneath the oceanic crust of the North American Plate.

5. Results

Event	Bin	Bounce point Longitude	Bounce point Latitude	SS Amplitude	G-Depth (km)	Uncertainty	G Amplitude	410 Depth (km)	410 Amplitude	660 Depth (km)	660 Amplitude
6/7/2015	1927	307.6564	26.276	1.30E+07	104.87	-7.625	-1.71E+05	408.69	2.30E+05	652.3	2.45E+04
6/7/2015	1966	309.9534948	25.89393355	5.13E+07	110.81	-6.285	-3.49E+05	406.57	2.50E+05	649.2	6.47E+04
5/24/2015	1592	299.1467396	12.48082526	5.47E+06	117.35	2.635	-3.05E+05	399	3.70E+04	N/A	N/A
5/24/2015	1721	303.335575	22.01121	4.16E+05	98.64	-5.27	6.95E+03	N/A	N/A	663.95	-5.18E+03
5/24/2015	1927	316.3419849	39.42457699	1.07E+05	96.5	-1.31	-1.40E+05	389.95	3.90E+03	632.6	1.23E+03
5/24/2015	1966	321.2103847	40.00164496	9.19E+05	98.04	-3.92	-7.20E+03	419.2	4.41E+03	642.5	1.88E+03
3/29/2014	1966	309.1233549	44.9219932	1.05E+06	101.57	6.715	5.85E+03	417.12	1.90E+04	669.8	4.74E+03
3/29/2014	1967	308.9552813	46.06737459	6.66E+05	103.01	2.67	5.29E+03	415.95	4.80E+03	N/A	N/A
11/22/2008	1722	302.2990766	26.80562953	3.53E+05	94.97	4.045	-4.90E+03	N/A	N/A	657.5	-2.40E+02
11/22/2008	1781	304.7683194	33.42921566	5.08E+06	95.31	4.03	-3.50E+03	400.1	3.30E+03	653.4	-1.26E+03
11/22/2008	1780	306.4450477	34.62234173	5.27E+05	92.01	-0.04	7.09E+03	400.6	1.40E+03	658.2	4.15E+03
8/28/2008	1927	314.6353824	48.88964816	1.10E+06	113.46	-6.685	-4.56E+04	N/A	N/A	653.4	-5.90E+03
8/28/2008	1966	314.3616484	49.07076642	9.46E+05	104.63	-9.325	-1.95E+04	416.3	-4.12E+03	652.8	-7.10E+03
4/24/2008	1927	306.8740996	44.15747896	8.00E+05	116.4	-4	2.70E+04	392.8	3.42E+04	662.1	-1.29E+03
4/24/2008	1966	307.656395	44.37619517	-5.43E+05	115.5	3.855	1.09E+05	398.2	2.96E+04	674.7	3.04E+03
5/4/2007	1781	304.9882504	33.9206198	1.98E+08	116.78	1.3	-4.60E+06	402.5	1.11E+04	N/A	N/A
5/4/2007	1722	302.8518008	31.48130045	1.86E+07	105.23	0.105	-1.51E+06	404.79	2.12E+05	638.7	1.19E+06
5/4/2007	1835	305.3898935	35.06426701	9.73E+06	122.97	0.195	-2.49E+05	N/A	N/A	647.8	-1.25E+05
5/4/2007	1721	302.7315133	32.3124479	8.91E+06	111.01	1.395	-5.45E+05	403.12	9.70E+04	633.15	5.25E+05
5/4/2007	1836	305.5616495	34.09891349	6.01E+06	121.07	-2.175	-5.50E+05	407.8	6.40E+04	623.6	2.80E+04
5/4/2007	1967	322.1201297	48.82696567	4.71E+05	122.44	-5.375	-1.70E+04	401.2	6.40E+04	623.9	1.50E+05

Table 2: Information regarding the 21 bins used, showing the sampled location, the depths and amplitudes of the picked precursors, and the uncertainty associated with them. Longitude and latitude information is in decimal degrees.

The depth, amplitude and uncertainty data in table 2 came from picks made on the resolved vespagram diagrams. The SS amplitude was used to normalize the other precursory amplitudes. The uncertainty was found by looking at the variation in the vespagrams on slowness's about 2 seconds per degree above and below the expected slowness for the G precursor. I picked the same peak in the above and below slowness's as the one in the predicted slowness. The offset of these peaks gave me a good estimate of how well I could resolve the pick.

6. Discussion

In order to visualize the depths of the precursors found in table 2, I created several maps seen in figure 4.1. These maps show the locations and relative depths of the bounce points at the G, 410 km, and 660 km discontinuities. Analyzing these maps left me with several conclusions. By looking at the maps designated for the depths of the 410 km and 660 km discontinuities, there is very little vertical variation. The maximum depth variation in the 410 km discontinuity was ±15 km. The maximum depth variation in the 660 km discontinuity was ±25 km. These results link closely with the results found in Gu et. al. (1998) and Shearer (1998). In those papers they concluded the 410 km and 660 km discontinuities have very little vertical variation and are global features. My results support this finding as these discontinuities were in fact found in the oceanic crust of the North American plate. By observing the map of the G, we see that this has even less variation in its depth, ±15 km. These results must be correlated to crustal age in order to make an assessment on the accuracy of my hypothesis.

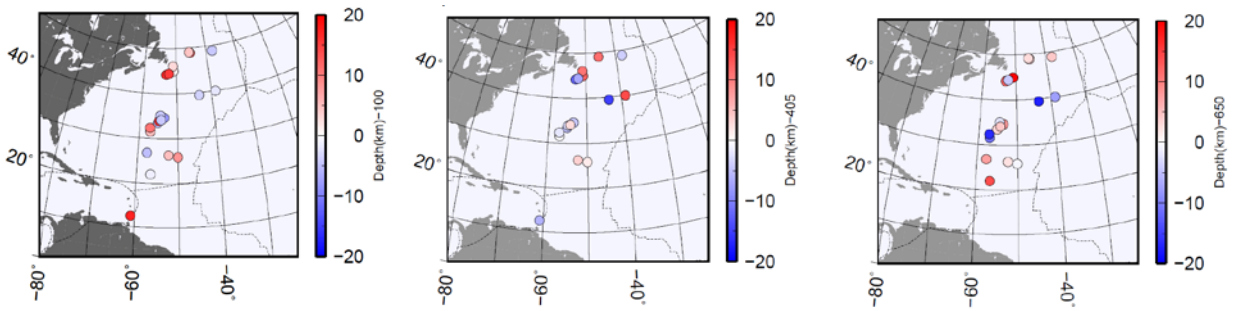

Figure 4.1 Plotted on these maps are the relative depths of the G, 410 km, and 660 km discontinuities.

To better understand the range distribution for these depths, I created the histograms seen below in figure 4.2. These histograms show the range of depths that I picked for each boundary, along with the range of the precursory amplitudes used to normalize SS. The depths for the G found in this study range from 90 km to 125 km. The depths for the 410 km discontinuity found in this study range from 390 km to 420 km. The depths for the 660 km discontinuity found in this study range from 625 km to 675 km.

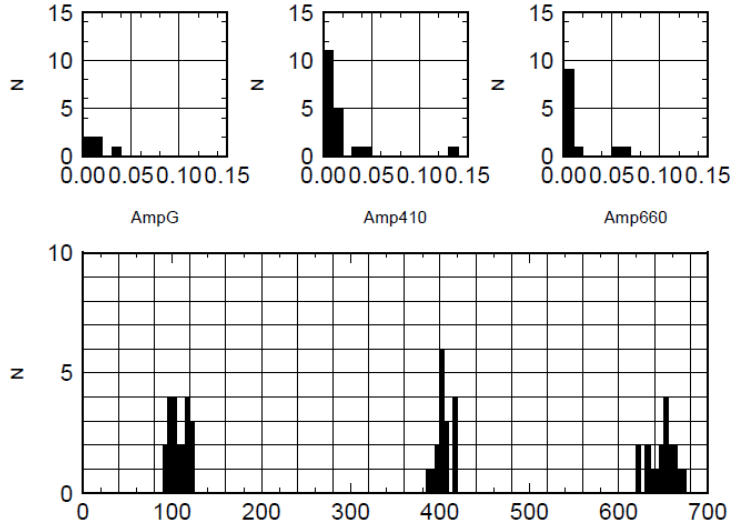

Figure 4.2 Top: Histogram showing the range of amplitudes used to normalize SS. Bottom: Histogram showing the range of depths for the G, 410 km and 660 km discontinuities.

The results of this study indicate that there is a good detection of the Gutenberg discontinuity beneath the oceanic crust of North America. When I compared these results to that of the results found Schmerr's (2012) study of the G beneath the Pacific Ocean, there is a considerable difference. He showed detections the seismic discontinuity from 50-80 km depth. My results show a much deeper detection of the discontinuity. His study does hold similar to mine in respect to the consistency of little variation in the depths.

To correlate the depths of the G with crustal age, I plotted the depth of the G against overlying crustal age. I showed this by using two different models for the thermal evolution of the oceanic lithosphere, seen in figure 4.3. The top plot shows the isocontours of temperature for a half space cooling model, where the plate increasingly thickens as it ages. The bottom plot is for a plate

model which specifies the equilibrium of the mantle and overlying lithosphere, meaning the thermal contours flatten at a particular age. By looking at the distribution of these points, I conclude that there is no correlation between the depth of the G and the overlying crustal plate age. As the overlying crustal age increases, we see no change in this range. This effectively invalidates my hypothesis that the Gutenberg discontinuity follows the lithosphere-asthenosphere boundary. I predict that this difference is caused by other factors. It is reasonably possible that this difference is caused by the presence of seismic anisotropy and/or compositional variation in xenoliths from the mantle. However, more data is necessary to resolve these predictions.

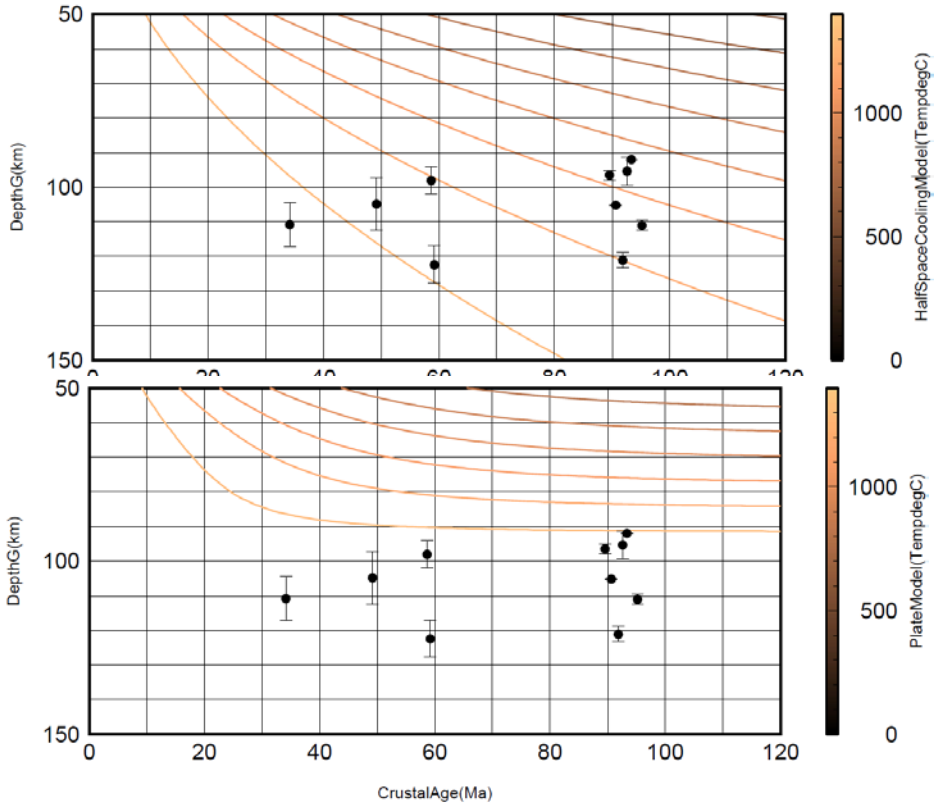

Figure 4.3 The X-axis shows the crustal age in Ma and the Y-axis shows depth in km. Top: shows the isocontours of temperature for a half space cooling model. Bottom: Shows the isocontours of temperature for a plate model.

To further this research, more seismic data will need to be collected. This can be done by adding earthquake events that occur in areas that sample beneath the oceanic crust of North America, typically occurring on the Atlantic mid ocean ridge area. This study helped show that the analysis of SS precursors can accurately determine depths of seismic discontinuities. Continuing to sample the depths of the G in parts of the world that have not yet been studied are important to furthering the information we have on the discontinuity.

8. Bibliography

Anderson, D., Sammis, C. Partial melting in the upper mantle. Physics of the Earth and Planetary Interiors, 3, 41. (1970).

Beghein, C., Yuan, K., Schmerr, N. & Xing, Z. Changes in Seismic Anisotropy Shed Light on the Nature of the Gutenberg Discontinuity. Science 343, 1237–1240. (2014).

DiVenere, Vic. Earth and Environmental Sciences. Introduction to Earth Sciences I. Mid Ocean Ridges. Columbia University. http://www.columbia.edu/~vjd1/MOR_basic.htm (2013)

Duess, A. Global Observations of Mantle Discontinuities Using SS and PP Precursors. Surveys in Geophysics, 30, 301-326. (2009).

Fischer, K., Ford, H., Abt, D., Rychert, C. The Lithosphere-Asthenosphere Boundary, Annual Review of Earth and Planetary Sciences, Vol. 38, 551-575. (2010)

Flanagan, M., Shearer, P. Global mapping of topography on transition zone velocity discontinuities by stacking SS precursors. Journal of Geophysical Research, 103, 2673-2692. (1998).

Gu, Y., Dziewonski, A., Agree, C. Global de-correlation of the topography of transition zone discontinuities. Earth and Planetary Science Letters, 157, 57-67. (1998).

Gu, Y., Dziewonski, A., Ekstrom, G. Preferentia; detection of the Lehmann discontinuity beneath continents. Geophysical Research Letters, 28, 4655-4658. (2001).

Hamza, V., Vieira, F., (2012), Global distribution of the lithosphere-asthenosphere boundary: a new look. Solid Earth, 3, 199–212. (2012).

Heit, B., Yuan, X., Bianchi, M., Kind, R., Gossler, J. Study of upper mantle discontinuities beneath eastern Asia by SS precursors. Geophysical Journal International, 183, 252-266. (2010).

Houser, C., Masters, G., Flanagan, M., Shearer, P. Determination and analysis of long-wavelength transition zone structure using SS precursors. Geophysical Journal International, 174, 178-194. (2008).

Karato, S., Jung, H. Water, partial melting and the origin of the seismic low velocity and high attenuation zone in the upper mantle. Earth and Planetary Sciences Letters, 157, 193. (1998).

Katrato, S., Wu, P. Rheology of the upper mantle: a synthesis. Science, 260, 771-778. (1993).

Rychert, C., Fischer, K., Rondenay, S. A sharp lithosphere–asthenosphere boundary imaged beneath eastern North America. Nature International weekly Journal of Science, 436, 542-54., (2005).

Rychert, C., Schmerr, N., Harmon, N., The Pacific Lithosphere-Asthenosphere Boundary: Seismic imaging and constraints on anisotropy from SS waveforms, Geochemistry, Geophysics, Geosystems, 13, doi:10.1029/2012GC004194. (2012).

Rychert, C. A., Harmon, N. & Schmerr, N. Synthetic waveform modelling of SS precursors from anisotropic upper-mantle discontinuities. Geophysical Journal International 196, 1694–1705. (2014).

Schmerr, N., The Gutenberg Discontinuity: Melt at the Lithosphere-Asthenosphere Boundary, Science, 335, 1480-1483. (2012).

Schmerr, N., Thomas, C., Subducted Lithosphere beneath the Kuriles from Migration of PP Precursors, Earth and Planetary Science Letters, 311, 101-111. (2011).

Schmerr, N., Garnero, E., McNamara, A. Deep mantle plumes and convective upwelling beneath the Pacific Ocean. Earth and Planetary Science Letters, 294, 143-151. (2010).

Schmerr, N., Garnero, E. Investigation of upper mantle discontinuity structure beneath the central Pacific using SS precursors. Journal of Geophysical Research, 111, B08305. (2006).

Shearer, P. Seismic imaging of upper-mantle structure with new evidence for a 520-km discontinuity. Nature, 344, 121-126. (1990).

Shearer, P. Upper mantle discontinuities. Geophysical Monograph, 117, 115-131. (2000).